Spatial luminescence imaging of dopant incorporation in CdTe Films

Harvey Guthrey,[a)] John Moseley, Eric Colegrove, James Burst, David Albin,
Wyatt K. Metzger, and Mowafak Al-Jassim

National Renewable Energy Laboratory, 15013 Denver West Pkwy, Golden, Colorado 80401, USA

State-of-the-art cathodoluminescence (CL) spectrum imaging with spectrum-per-pixel CL emission mapping is applied to spatially profile how dopant elements are incorporated into Cadmium telluride (CdTe). Emission spectra and intensity monitor the spatial distribution of additional charge carriers through characteristic variations in the CL emission based on computational modeling. Our results show that grain boundaries play a role in incorporating dopants in CdTe exposed to copper, phosphorus, and intrinsic point defects in CdTe. The image analysis provides critical, unique feedback to understand dopant incorporation and activation in the inhomogeneous CdTe material, which has struggled to reach high levels of hole density. *Published by AIP Publishing.*
[http://dx.doi.org/10.1063/1.4974459]

I. INTRODUCTION

Cadmium telluride (CdTe) solar cells have recently achieved a record conversion efficiency of 22.1%[1] and are now cost competitive with fossil fuel electricity generation. Significant increases in CdTe cell efficiency over the last several years have resulted from increases in the short-circuit current density (J_{sc}) and fill factor; however, further efficiency gains require increasing the open-circuit voltage (V_{oc}). V_{oc} has not increased beyond the 840–890-mV range for champion-efficiency cells in the past two decades and offers room for improvement.[1,2] One reason for this situation is the generally low hole densities in polycrystalline CdTe devices. Theoretical studies of CdTe doping have attributed low hole density to (1) compensation effects for both intrinsic and extrinsic dopants and (2) difficulty in finding dopant species with ideal combinations of solubility and defect levels.[3] However, recent efforts to enhance the charge-carrier density have successfully achieved higher values of V_{oc}, even exceeding 1 V in single-crystal CdTe.[4,5] To consistently produce CdTe devices with high V_{oc}, it is necessary to understand the fundamental mechanisms of incorporation and activation of different dopant species; and in polycrystalline devices, it is important to understand the roles of grain boundaries (GBs) and intra-grain (IG) defects. In this work, we focus on CdTe subjected to extrinsic doping involving Cu and P, and we also comment on intrinsic doping treatments in the large-grain material.

Phosphorus can act as a shallow acceptor when positioned on a Te site.[6–8] Although group V elements are typically difficult to incorporate into CdTe, P incorporation is one of the most favorable of this group depending on growth conditions.[3,8] Under Cd-rich conditions, as used in the present work, the compensating Cd_i defect can easily form; but the shallow acceptor level associated with P is likely to circumvent this effect depending on the position of the Fermi energy.[3] Calculations have confirmed that this configuration

has the lowest formation energy—again depending on the Fermi energy—and is most likely to behave as a negatively charged acceptor.[9] Multiple luminescence studies have focused on the CdTe:P material where the P was incorporated by diffusion,[6] ion implantation,[10,11] and chemical vapor processes.[12] These studies, using photoluminescence (PL) spectroscopy,[6,7,10,11] have definitively identified characteristic luminescence related to P_{Te} acceptor states with a zero phonon line at about 1.535 eV accompanied by phonon replicas. These measurements were not spatially resolved due to the spot size of the excitation source relative to structural defects in the CdTe material. Grain boundaries are believed to play a major role in incorporating P into CdTe films, and recent work with time-of-flight secondary-ion mass spectrometry (TOF-SIMS) has directly measured enhanced P at grain boundaries.[9] A cathodoluminescence (CL) study, where the excitation source was small enough to resolve individual defects, found "bright" contrast at structural defects, but spectra were not obtained to confirm the nature of the increased CL signal.[12] An un-doped sample in that study exhibited only dark contrast at structural defects. Observing different contrasts at structural defects provides insight into the dominant recombination mechanism and energy levels associated with a particular feature.[13,14] In terms of this work, "bright" means an enhanced CL signal and "dark" means a decreased CL signal relative to adjacent areas.

Another influential extrinsic dopant investigated in this work is Cu, which can contribute to charge-carrier concentration through the Cu_{Cd} acceptor. However, like P, the incorporation of Cu depends on the growth conditions and prefers a Te-rich condition to suppress the self-compensation of the Cu_i species that is favored under Cd-rich conditions.[3] Various PL studies have focused on Cu-doped CdTe and have identified the luminescence characteristic of transitions involving Cu_{Cd} as well.[6,15,16] Understanding the mechanism by which Cu is incorporated is particularly important because the back-contact material typically contains Cu, which can migrate into the CdTe absorber layers, making

---

a)Author to whom correspondence should be addressed. Electronic mail: harvey.guthrey@nrel.gov

this a global issue for CdTe devices. Calculations have shown that the increased Cu content can result in higher or lower hole densities depending on the concentrations.[17] Determining how Cu interacts with extended defects may provide insight into CdTe doping and performance.

The results presented here build on earlier PL studies by spatially resolving the variations in emission that are characteristic of particular dopant species. We use low-temperature CL, which can reveal dopants spatially by tracking the emission intensity of characteristic luminescence peaks. This is one of the few techniques that allow spatial resolution and analysis of key point defects such as Cu_{Cd} and P_{Te} throughout the device. Observing P- and Cu-containing samples in both plan-view and cross-section orientation provides information on the role that extended defects have on dopant incorporation.

II. EXPERIMENTAL

To study spatial variations in dopant incorporation, we used two types of CdTe: (1) large-grain CdTe samples grown by the Bridgman technique with grain diameters on the order of 1 mm and (2) CdTe films grown by close-spaced sublimation (CSS) with grain diameter ranging from several microns at the growth interface to 10–15 microns at the surface. The large-grain and CSS samples were compared separately although some connections between the different analyses will be discussed. The motivation for working with grain sizes much larger than typical CdTe films used in photovoltaic (PV) devices (~several microns) was to be able to easily distinguish the CL signal originating from grain boundaries (GBs) and from grain interiors (GIs). Large grains reduce the potential for interaction with multiple defect features, and thus, the CL signal is dominated by specific defects. The majority of previous work has been on CdTe with typical grain sizes of a few microns, so this approach acts to reduce any uncertainty in the origin of observed recombination behavior. Each set of samples underwent different treatments with the aim of increasing the hole density, with the as-grown material included for comparison.

The treatments for the large-grain samples are as follows. The P-diffused sample is prepared by annealing Cd + P in a closed ampoule; this anneal provides both the P dopant and the Cd overpressure to encourage P substitutional doping on Te sites. The Cu-diffused sample is prepared by first depositing a Cu film onto the surface, followed by annealing in a diffusion furnace. The Te-anneal sample is annealed in a closed ampoule with Te, and the Cu-diffused + Te-anneal combines the diffusion of the Cu film followed by the Te anneal in a closed ampoule, which serves to diffuse Cu and activate the Cu on Cd sites, respectively. The CSS samples only underwent the P and Cu diffusion treatments under similar conditions to the large-grain samples.

CL analysis of the larger-grain bulk samples was performed on a JEOL JSM-5800 scanning electron microscope (SEM) operating at an accelerating voltage of 7-kV, a beam current of ~1 nA, and a temperature of 25 K. Spectra were collected with a Princeton Instruments 2560i spectrograph equipped with a liquid-nitrogen-cooled Si charge-coupled

device (CCD) detector. The smaller-grain samples were analyzed in cross-section in a JEOL JSM-7600 field-emission SEM (FESEM) operating at an accelerating voltage of 5-kV, a beam current of ~1 nA, and a temperature of 6 K. CL spectra were collected with a Horiba CLUE system equipped with a Peltier-cooled Sincerity Si CCD. The backscattered electron images were acquired in this system with an accelerating voltage of 10 kV and a beam current of ~1 nA. In both systems, the electron-beam scanning is synchronized with the spectrum collection so that an entire CL spectrum is acquired for each pixel in the scan region. The spectra can then be extracted individually from features of interest (e.g., GBs, GIs, and intra-grain (IG) defects) to study spatial variations in the CL emission from the sample. We also performed capacitance vs. voltage measurements on the smaller-grain samples to monitor the carrier concentration. Devices for C-V measurements were prepared in the standard CdTe superstrate device configuration (glass/SnO_2:F/SnO_2/CdS/CdTe:P/back contact). In order to prevent co-doping with Cu, the back contact for these devices was a Cu-free graphite paste (electro-DAG). C-V measurements were performed using a Hewlett Packard 4284A Precision LCR Meter (controlled with LabVIEW) at 50 kHz with an amplitude of 0.05 V and bias voltage swept from 0.5 to −1.5 V.

III. RESULTS AND DISCUSSION

CL total emission intensity images and profiles across grain boundaries are shown for the five bulk samples in Fig. 1. Due to the large grain diameter (~mm), specific grain boundaries can be imaged independent of others. The as-grown profile shows the CL emission intensity at the GBs decreasing relative to both adjacent GIs; additionally, there are a number of intra-grain defects that exhibit reduced CL intensity. This is an expected consequence of the energy levels introduced at these structural disruptions in the CdTe crystal that allow for efficient non-radiative carrier recombination.

The sample subjected to P incorporation appears very different from the as-grown sample. Again, the GB in this image exhibits a very low CL intensity; but in Fig. 1(b), the CL intensity increases significantly immediately adjacent to the GB. This effect has been observed in a previous CL study of P-doped CdTe.[12] The spectra for this sample do not resemble typical high-efficiency CdTe emission. Instead, these spectra closely match that of a P-doped sample annealed under a high cadmium overpressure[8] in a previous study. There is no detectable excitonic emission and only one broad peak centered at ~1.46 eV both at and away from the GB. This suggests that the P in this sample is not in the P_{Te} configuration, but rather, it creates a deeper energy level that acts as an efficient recombination center, which reduces emission intensity.

Insight into the luminescence in this sample can be gained by comparison with a GB in a P-diffused sample in cross-section. Figure 2 is the spectra from the sample in Fig. 1(b) compared in Fig. 2(b) with that from a GB indicated in Fig. 3. The spectra are quite similar—in particular, no exciton luminescence is observed, and there is one broad peak centered around the 1.46–1.5-eV range. If P were sitting on
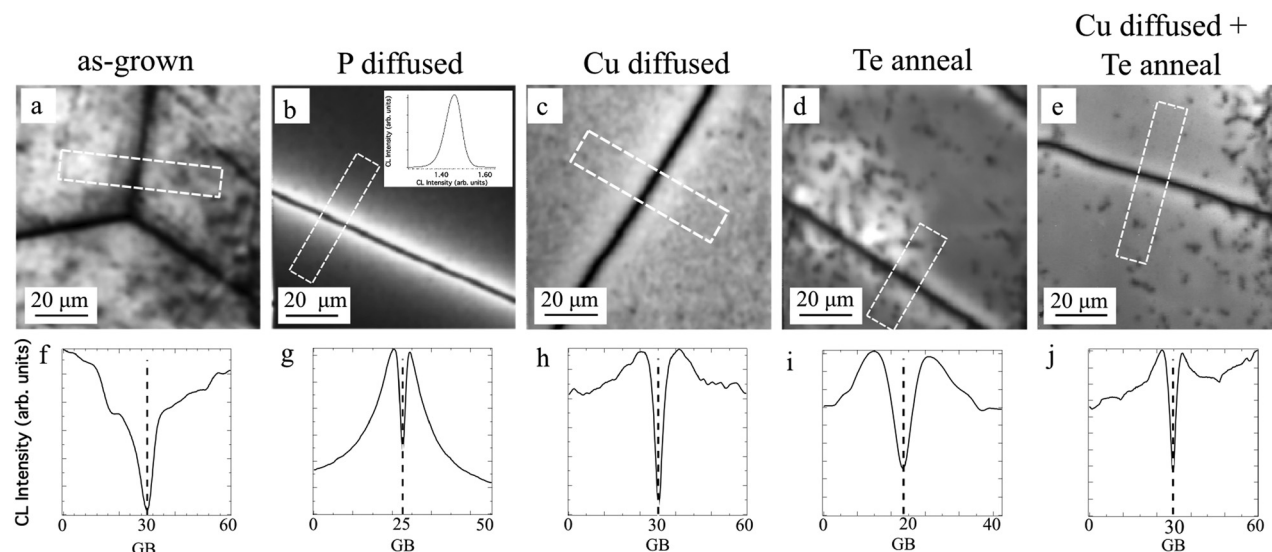
FIG. 1. (a)–(e) CL images created from emission between 750 and 1000 nm. (f)–(j) Averaged CL intensity profiles taken across the grain boundaries are visible in (a)–(e). The dashed lines indicate the GB positions. Intensity scales for images are specific to each individual image to highlight relative variations and cannot be used for directly comparing emission intensity.

the Te site as intended, we would expect excitonic emission and a peak at about 1.535 eV accompanied by phonons. The lack of this type of emission suggests that P is in such high concentration that the lattice is distorted from the CdTe crystal structure. The lack of phonon replicas supports this because they depend on coupling between the defect species and the crystal lattice. The similarity of the surface (Fig. 2(a)) and the GB (Fig. 2(b)) also supports the idea of two different diffusion mechanisms.[9] Surfaces, internal (GBs) or external, that are associated with the drive-in diffusion process should contain higher concentrations of P than the surrounding bulk material and appear electronically similar. Subsequent heat treatments would then allow this P to move into the surrounding regions and occupy the Te site as intended.

Although not as dramatic as the P-diffused sample, the Cu-diffused sample shows a similar enhancement of the CL signal adjacent to the GB (Figs. 1(c) and 1(h)). Cu diffusion into CdTe has been shown to alter GB recombination behavior;[18] the Cu-diffused + Te-annealed and Te-annealed samples show similar behavior to the Cu-diffused sample that was also annealed in a Te overpressure, as indicated by the intensity profiles in Figs. 1(i) and 1(j). There appears to be a difference in the degree to which the GB emission is reduced relative to the remote grain interiors; however, because of the limited dataset, it is not possible to state whether or not this is a global trend for these treatments. An interesting observation is that there are intra-grain defects visible (dark spots) in these three samples but not in the P-diffused sample. Since the dark spots are more prevalent in the as-grown sample that was not exposed to any excess Te treatments, they are not believed to be a result of Te precipitates but are likely due to structural defects within the GIs.

At this point, we focus on the regions adjacent to the grain boundaries. Similar observations have been made in silicon using electron-beam-induced current, where distinct regions around GBs exhibited enhanced carrier collection;

this was attributed solely to a gettering action by the GB that removed impurities from the surrounding regions.[20] We believe that this is not the case for these samples because such a silicon material already contains the impurities whose position is influenced by the GB, and in these CdTe samples, we are looking at the inverse process. The impurities are incorporated through the grain boundary[9] and can then diffuse away from the GB, resulting in a higher concentration near the GB. Thus, a plausible explanation for the increased CL intensity surrounding GBs arises by considering the factors affecting CL emission in CdTe—namely, the concentration of donors and acceptors. The CL emission intensity depends on changes in the concentrations of free electrons and holes, excitons, and ionized, as well as neutral donor and acceptor species. An increase in the concentration of shallow-level defects surrounding GBs—to some "optimum" value in terms of radiative recombination probability—would explain the increase in CL intensity observed in these samples. It is also possible that the GB potentials arising from compositional variations influence electron-hole transport and affect the local recombination and CL intensity. However, we would expect these potentials largely to be screened by the injected carriers. Using rate equations to model the CL emission has proven effective in understanding the changes in intensity and emission spectra in CdTe.[21]

An example of this is shown in Fig. 3. Here, we see a CL intensity image (Fig. 3(a)) for a P-diffused sample in cross-section orientation. Experimental spectra (Fig. 3(b)) for three points near the boundary (indicated in Fig. 3(a)) show a significant increase in the P_{Te} emission. Using the rate equation model, the simulated spectra in Fig. 3(c) are meant to show the effect of increased P_{Te} acceptor concentrations on the CL emission. These spectra differ only in the value (X) of acceptor concentration, and clearly, an increase in this acceptor concentration would result in spectra similar to that of Fig. 3(b). Details of this model are given in Ref. 21. A comment should be made regarding the relative

Experimental Spectra
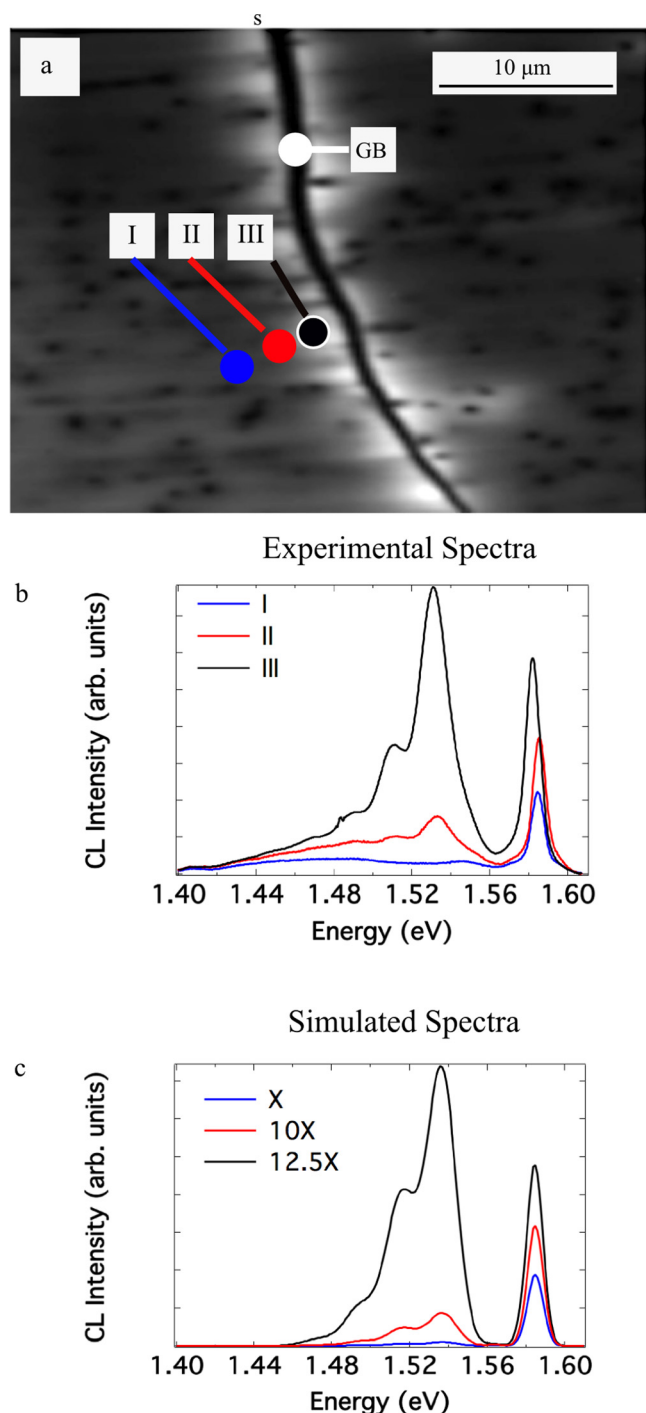

Simulated Spectra

FIG. 2. (a) CL spectra from a P-diffused sample in plan-view and (b) CL spectra from a GB in a P-diffused sample in cross-section showing the similarity of the luminescence.

P-diffused Sample Plan-View

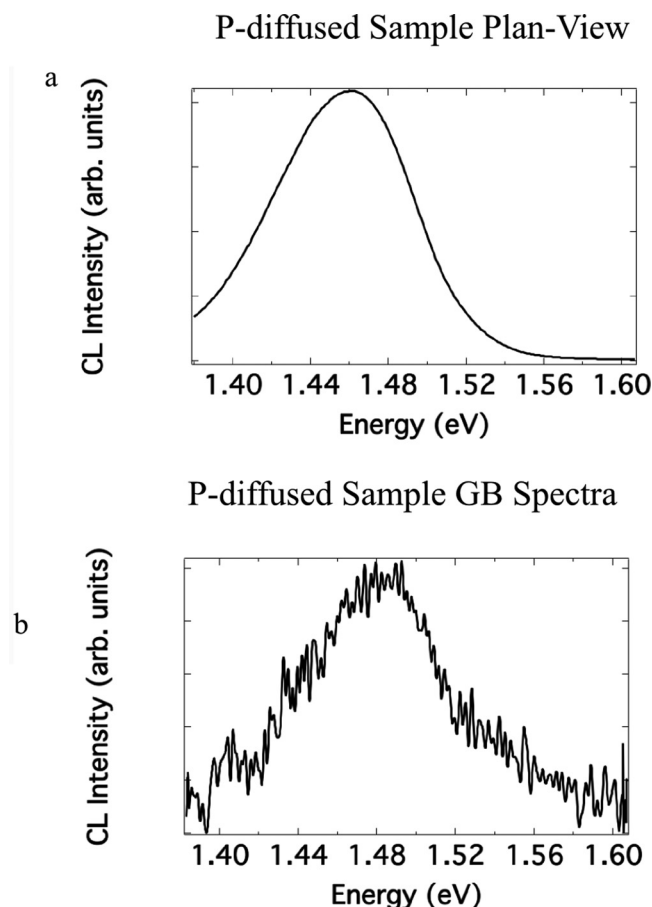

P-diffused Sample GB Spectra

FIG. 3. (a) The CL intensity image of a P-doped CdTe film in cross-section, (b) experimental spectra from the three points indicated in (a) showing the significant change in emission related to the P_{Te} transition, and (c) simulated spectra using a rate equation model demonstrating that the acceptor concentration, X, strongly influences the intensity of defect emission in CdTe.

intensities of the peaks. In Ref. 21, the increase in shallow acceptors increased the deeper emission, but the relative intensity of the exciton emission was reduced. The competing recombination mechanisms responsible for changes in the emission intensity of peaks relative to one another depend strongly on the chemistry of a particular sample. This is likely why the same relative decrease in the exciton is not observed in the spectra in Fig. 2.

We now focus on the cross-section analysis of CSS-deposited films with smaller grain size than the preceding

sample set. The cross-section CL analysis on the smaller-grain CdTe film allows us to visualize doping throughout the sample thickness. We can connect the spatial distribution of P in the film with the GBs by using the backscattered electron images (Figs. 4(a)–4(c)), false-color CL images (Figs. 4(d)–4(f)), and averaged spectra (Figs. 4(g)–4(i)) for an as-grown untreated sample and different regions of the same film after P diffusion and P diffusion with activation. The color scheme for the false-color images is indicated in the averaged spectra plots; and being consistent for each image, it is intended to qualitatively highlight the differences in the dominant emission in different regions of the samples. The color of the images is meant to indicate the dominant emission: blue for excitons, green for P_{Te} transitions, and red for deeper-level transitions. The averaged spectra for each sample show that the relative intensity of the different emission peaks differs significantly for each sample. The as-grown sample exhibits only excitonic emission accompanied by deeper emission that is typical of as-grown CdTe.

In the P-diffused sample, the excitonic emission is dominant in the grain interiors and also visible is the peak accompanied by the characteristic phonon replicas (previously identified in multiple PL studies[7,8,11] at about 1.535 eV). This peak associated with the P_{Te} transition contributes to the green
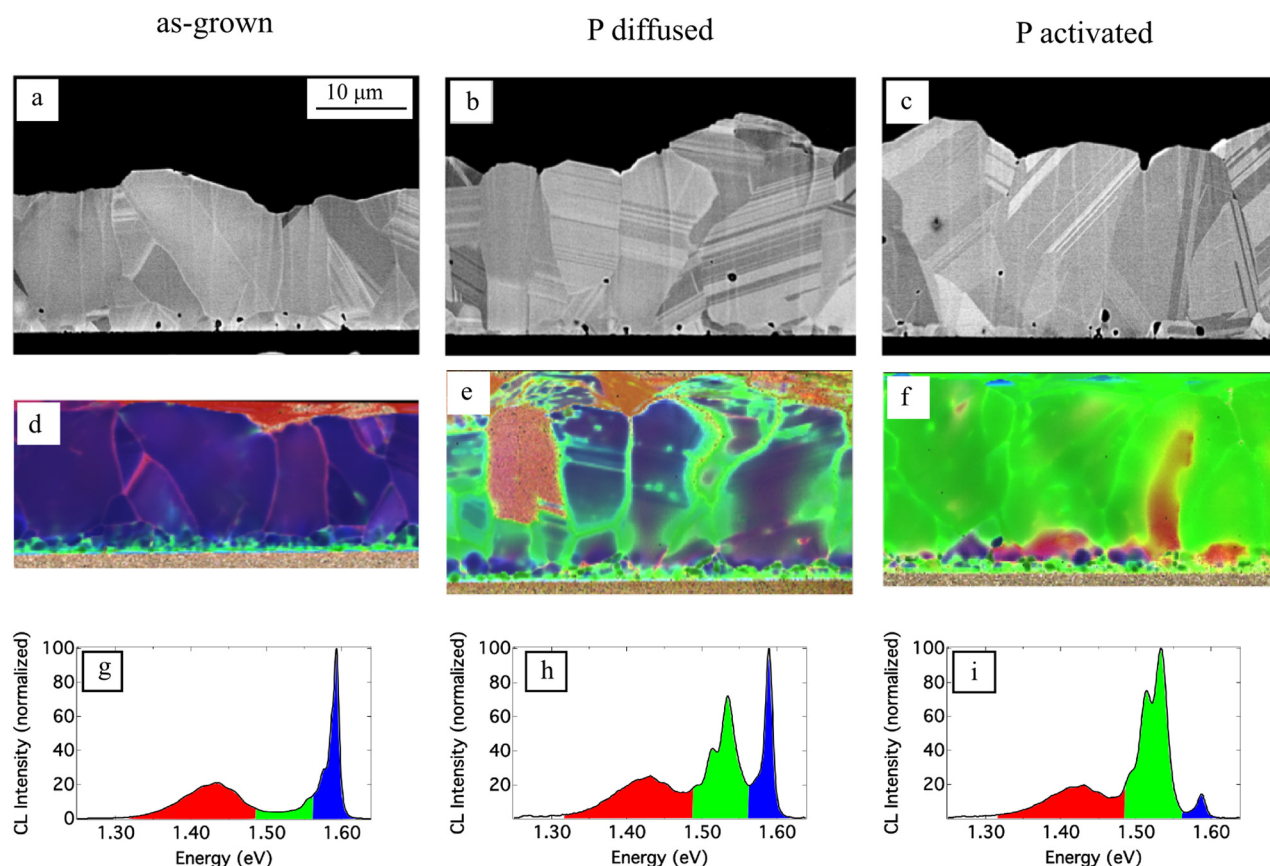
FIG. 4. (a)–(c) Backscattered electron images, (d)–(f) false-color CL images, (g)–(i) averaged CL spectra for the same CdTe film after different P treatments. The color scheme for the false-color images is indicated in the averaged spectra plots and is intended to qualitatively highlight the differences in the dominant emission in different regions of the samples.

regions in the false-color images (except for the as-grown sample) and is clearly concentrated around GBs. After activating samples in a Cd overpressure at $500\,^{\circ}\mathrm{C}$ for 5 min, the averaged spectra show a significant increase in the P_{Te} emission that dominates the entire film. We notice that the P_{Te} peak is no longer confined to regions around GBs because, from the false-color image, it is clearly the dominant emission throughout the majority of the grain interiors—in stark contrast to the sample that did not undergo activation. This provides a clear illustration shifting P, which was likely present in the grain interiors in a non-radiative point defect state observed by capacitance but not luminescence, onto Te sites.[9] We expect the presence of the P_{Te} species through a greater volume of the CdTe film to translate to a higher hole concentration, and this was confirmed through capacitance vs. voltage measurements as shown in Fig. 5. The hole concentration increases more than two orders of magnitude from the as-grown state and about one order of magnitude from the P-diffused state, where there was no further P addition during the activation process.

Similar analysis can be applied to Cu, another critical acceptor dopant. Results of cross-section CL analysis on Cu-diffused and Cu-activated samples are shown in Fig. 6. Looking at the CL false-color image (Fig. 6(c)) of the Cu-diffused sample, there is an interesting contrast to the P-diffused sample. All film regions are dominated by exciton-related emission. The emission peak associated with the

Cu_{Cd} defect is prominent but weak relative to the exciton peak, and the distribution of this emission is more uniform over the film than the P-diffused sample, where the P_{Te} acceptor peak was clearly visible and concentrated around GBs. There appears to be an increase in the CL signal around most grain boundaries; but from the relative intensities of the exciton and deeper emission, it was unclear from looking at individual spectra whether this is solely due to an increase in
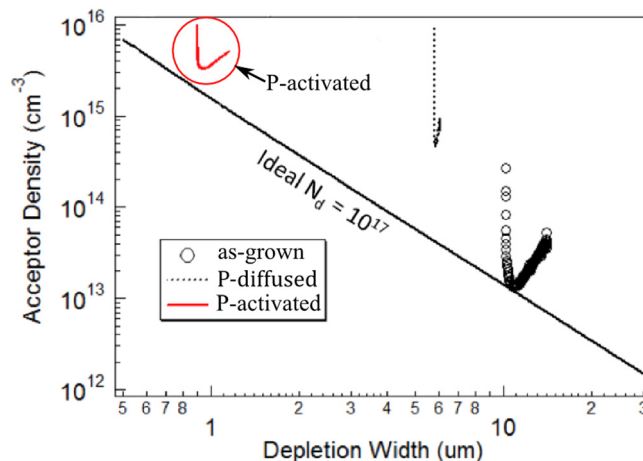

FIG. 5. Results of capacitance vs. voltage analysis showing the increase in P_{Te} acceptor concentration after both the P diffusion and P activation treatments.
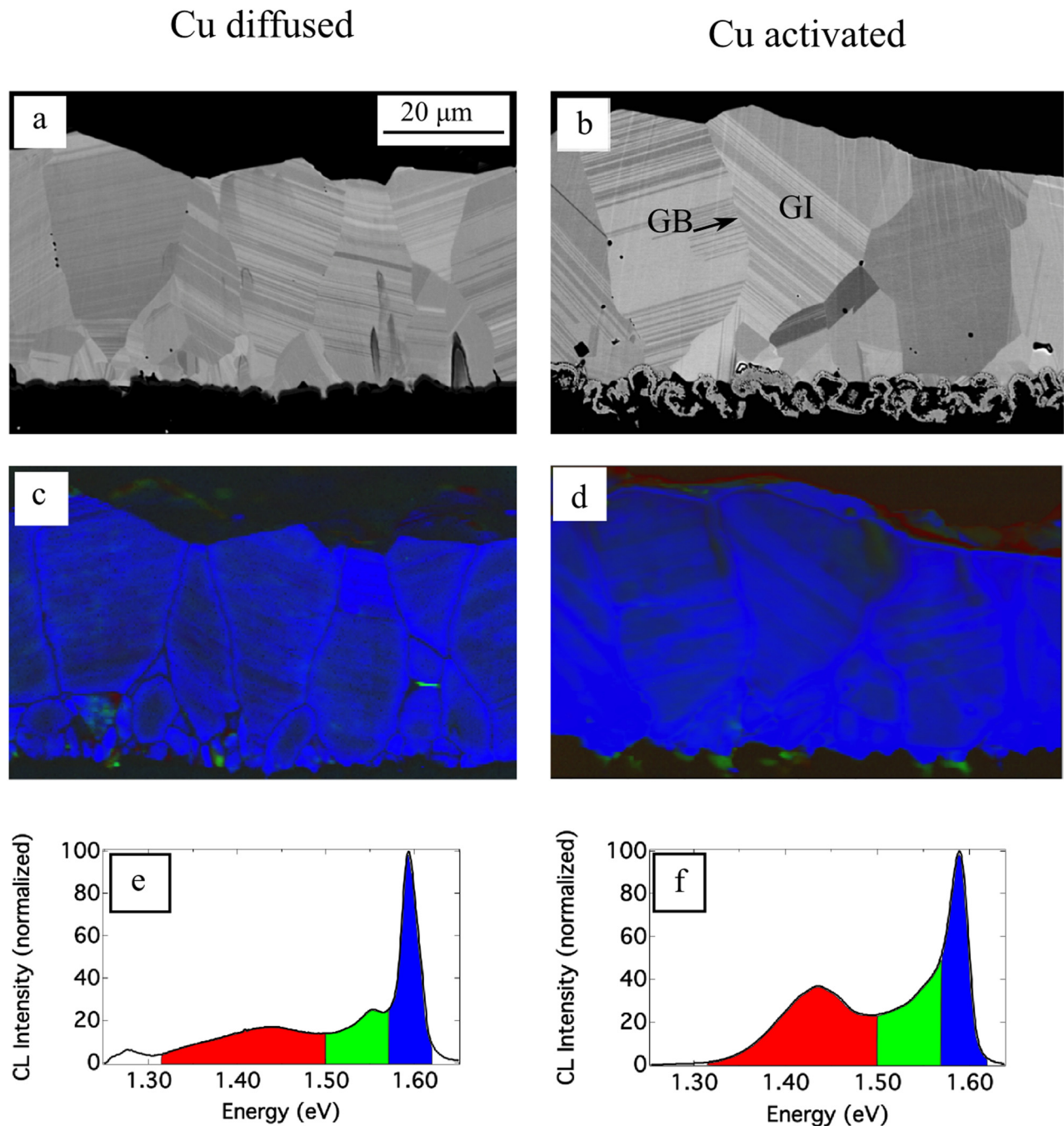
FIG. 6. (a) and (b) Backscattered electron images, (c) and (d) false-color CL images, and (e) and (f) averaged CL spectra for the same CdTe film after different Cu treatments. The color scheme for the false-color images is indicated in the averaged spectra plots and is intended to qualitatively highlight the differences in the dominant emission in different regions of the samples.

the Cu_{Cd} acceptor concentration. In the Cu-activated sample, there is a broad emission peak originating from a zero-phonon peak at 1.45 eV that corresponds to Cu_{Cd}.[6,16,22–28] Although the exciton emission still dominates in all regions of the film, the GB spectra indicated a clear increase in the Cu_{Cd} concentration as shown in Fig. 7. These spectra are normalized to show the difference in relative intensity of the exciton and Cu_{Cd} emission. This is in contrast to the P-activated sample because the Cu_{Cd}-related emission was not as evenly distributed after the activation process.

The GBs appear dark in all of the bulk samples as well as the cross-section samples. CL images for the latter in

Figs. 4 and 6 were normalized to show the type of emission present, rather than the change in intensity. It is reasonable to assume a reduced CL intensity at GBs because there are high concentrations of deep-level defects that are likely to act as non-radiative recombination centers. In fact, the line profiles in Fig. 1 show that the GBs in all of these samples exhibit reduced CL emission relative to the GIs. Note that similar profiles could be produced from the cross-section samples in this study, as well. It is reasonable to assume that reduced GB CL intensity is caused by higher concentrations of deep-level defects that act as non-radiative recombination centers. Some previous work suggested that Cl and Cu can
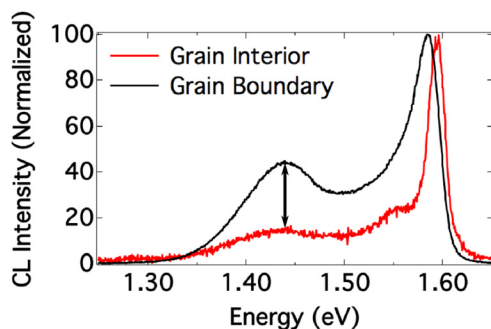
FIG. 7. Normalized CL spectra from a grain boundary and grain interior in the Cu-activated sample as indicated in Fig. 5(b), showing the difference in relative intensity of the Cu_{Cd} emission at the GB.

reduce recombination at GBs in CdTe.[19] Previous CL studies have shown that although Cl can reduce GB recombination, total passivation is not likely.[29] Our observations suggest that the treatments here also do not result in total GB passivation; more statistical studies would be needed to quantify and compare GB passivation. What is clear from these observations is the alteration of the regions around GBs in terms of charge-carrier concentration.

IV. SUMMARY

In this work, we have demonstrated how CL spectrum imaging can be used to monitor the presence and spatial distribution of critical dopant species in the CdTe PV material. Enhanced CL emission from regions proximal to grain boundaries suggests higher concentrations of acceptor species, as shown in the application of rate-equation-based simulations used to explain our experimental results. Understanding how various dopants are integrated into the CdTe PV material, and if and how they are activated, will lead to tuning of the film morphology and optimization of incorporation processes. The tuning and optimization will both allow for increased V_{oc}, and ultimately, for higher efficiencies of PV devices based on polycrystalline CdTe absorbers.

ACKNOWLEDGMENTS

[1]M. A. Green, K. Emery, Y. Hishikawa, W. Warta, and E. D. Dunlop, Prog. Photovoltaics: Res. Appl. **24**, 3–11 (2016).
[2]M. A. Green and K. Emery, Prog. Photovoltaics: Res. Appl. **1**, 25–29 (1993).
[3]S.-H. Wei and S. Zhang, Phys. Rev. B **66**, 155211 (2002).
[4]J. M. Burst, J. N. Duenow, D. S. Albin, E. Colegrove, M. O. Reese, J. A. Aguiar, C.-S. Jiang, M. Patel, M. M. Al-Jassim, and D. Kuciauskas, Nat. Energy **1**, 16015 (2016).
[5]J. Duenow, J. Burst, D. Albin, D. Kuciauskas, S. Johnston, R. Reedy, and W. Metzger, Appl. Phys. Lett. **105**, 053903 (2014).
[6]J. M. Burst, S. B. Farrell, D. S. Albin, E. Colegrove, M. O. Reese, J. N. Duenow, D. Kuciauskas, and W. K. Metzger, APL Mater. **452**, 116102 (2016).
[7]E. Molva, J. Pautrat, K. Saminadayar, G. Milchberg, and N. Magnea, Phys. Rev. B **30**, 3344 (1984).
[8]J. Saraie, H. Shinohara, H. Edamatsu, and T. Tanaka, J. Lumin. **21**, 337–351 (1980).
[9]E. Colegrove, S. P. Harvey, J.-H. Yang, J. M. Burst, D. S. Albin, S.-H. Wei, and W. K. Metzger, Phys. Rev. Appl. **5**, 054014 (2016).
[10]E. Molva, K. Saminadayar, J. Pautrat, and E. Ligeon, Solid State Commun. **48**, 955–960 (1983).
[11]C. Kraft, A. Brömel, S. Schönherr, M. Hädrich, U. Reislöhner, P. Schley, G. Gobsch, R. Goldhahn, W. Wesch, and H. Metzner, Thin Solid Films **519**, 7153–7155 (2011).
[12]A. Alnajjar, C. Watson, A. Brinkman, and K. Durose, J. Cryst. Growth **117**, 385–390 (1992).
[13]L. J. Balk, Adv. Electron. Electron Phys. **71**, 1–73 (1988).
[14]B. G. Yacobi and D. B. Holt, *Cathodoluminescence Microscopy of Inorganic Solids* (Springer Science & Business Media, 2013).
[15]J. Chamonal, E. Molva, and J. Pautrat, Solid State Commun. **43**, 801–805 (1982).
[16]D. Kuciauskas, P. Dippo, A. Kanevce, Z. Zhao, L. Cheng, A. Los, M. Gloeckler, and W. K. Metzger, Appl. Phys. Lett. **107**, 243906 (2015).
[17]J. Ma, S.-H. Wei, T. Gessert, and K. K. Chin, Phys. Rev. B **83**, 245207 (2011).
[18]D. Mao, G. Blatz, C. Wickersham, and M. Gloeckler, Sol. Energy Mater. Sol. Cells **157**, 65–73 (2016).
[19]J. D. Poplawsky, N. R. Paudel, C. Li, C. M. Parish, D. Leonard, Y. Yan, and S. J. Pennycook, Adv. Energy Mater. **4**, 15 (2014).
[20]J. Lu, M. Wagener, G. Rozgonyi, J. Rand, and R. Jonczyk, J. Appl. Phys. **94**, 140–144 (2003).
[21]J. Moseley, M. M. Al-Jassim, H. L. Guthrey, J. M. Burst, J. N. Duenow, R. K. Ahrenkiel, and W. K. Metzger, J. Appl. Phys. **120**, 105704 (2016).
[22]W. Stadler, D. Hofmann, H. Alt, T. Muschik, B. Meyer, E. Weigel, G. Müller-Vogt, M. Salk, E. Rupp, and K. Benz, Phys. Rev. B **51**, 10619 (1995).
[23]E. Molva, J. Chamonal, G. Milchberg, K. Saminadayar, B. Pajot, and G. Neu, Solid State Commun. **44**, 351–355 (1982).
[24]J. Laurenti, G. Bastide, M. Rouzeyre, and R. Triboulet, Solid State Commun. **67**, 1127–1130 (1988).
[25]K. James, J. Merz, and C. Jones, J. Vac. Sci. Technol., A **6**, 2664–2669 (1988).
[26]F. Molva, J. Chamonal, and J. Pautrat, Phys. Status Solidi B **109**, 635–644 (1982).
[27]T. Kuhn, W. Ossau, A. Waag, R. Bicknell-Tassius, and G. Landwehr, J. Cryst. Growth **117**, 660–665 (1992).
[28]D. Grecu, A. Compaan, D. Young, U. Jayamaha, and D. Rose, J. Appl. Phys. **88**, 2490–2496 (2000).
[29]J. Moseley, W. K. Metzger, H. R. Moutinho, N. Paudel, H. L. Guthrey, Y. Yan, R. K. Ahrenkiel, and M. M. Al-Jassim, J. Appl. Phys. **118**, 025702 (2015).